# Embrittlement of an elasto-plastic medium by an inclusion

**Luca Cimbaro** · **Adrian P. Sutton** ·
**Daniel S. Balint** · **Anthony T. Paxton** ·
**Mark C. Hardy**

**Abstract** A mathematical model for the embrittlement of a long elastic-plastic crack by a relatively small, misfitting inclusion is presented. The model makes direct contact with the Dugdale–Bilby–Cottrell–Swinden model as a limiting case. The particular case of an oxide inclusion with a triangular cross-section at the tip of an intergranular crack in the Ni-based superalloy RR1000 at 650 °C is considered. The positive misfit of the intrusion provides an additional tensile load on the crack tip and on the plastic zone, raising the local stress intensity factor $k_I$ and the crack tip opening displacement $\Delta u$ above those when the inclusion is replaced by a dislocation-free zone of the same length. It is shown that for a given misfit strain and inclusion shape, the enhancement of $k_I$ and $\Delta u$ is controlled by a dimensionless parameter $\omega = (\sigma/\sigma_1)\sqrt{c/(2l)}$ where $\sigma$ is the applied stress, $\sigma_1$ is the yield stress, $c$ is the crack length and $l$ is the length of the inclusion. The anti-shielding effect of the intrusion is significant only when $\omega \lesssim 6$. As a result of the anti-shielding effect of the intrusion, the stress singularity at the crack tip always exceeds the compressive normal stress that exists within the thickest part of the intrusion when it is isolated. It is also shown that the gradient of the hydrostatic stress within the intrusion subjected to different applied stresses drives the oxygen diffusion and, hence, assists the oxidation at the grain boundary. The fracture toughness is considerably greater than that of a bulk sample of the oxide particle, which we attribute to the plastic zone.

L. Cimbaro · A. P. Sutton (✉)
Department of Physics, Imperial College London,
Exhibition Road, London SW7 2AZ, UK
e-mail: a.sutton@imperial.ac.uk

D. S. Balint
Department of Mechanical Engineering, Imperial College London, Exhibition Road, London SW7 2AZ, UK

A. T. Paxton
Department of Physics, King's College London, Strand, London WC2R 2LS, UK

M. C. Hardy
Rolls-Royce plc, P.O. Box 31, Derby DE24 8BJ, UK

## 1 Introduction

When a brittle inclusion forms at a loaded crack tip it may enhance the growth of the crack by providing a path of relatively low fracture energy. An important example is the embrittlement of Ni-based superalloys due to environmental oxygen at temperatures around 700 °C in rotor discs of gas turbine engines. At low temperatures, the fatigue crack growth is transgranular and is caused by localised plastic deformation at the crack

tip (Liu and Oshida 1986; Andrieu et al. 1992; Bache et al. 1999; Knowles and Hunt 2002; Li et al. 2015; Cruchley et al. 2015a, b; Németh et al. 2016; Hörnqvist et al. 2014). But at temperatures around 700 °C in an oxidising environment, the mode of fracture changes to intergranular. In this case oxygen enters the crack tip, diffuses along a $\gamma/\gamma$ or $\gamma/\gamma'$ interface and reacts to produce an oxide particle called an intrusion (McMahon and Coffin 1970; Andrieu et al. 1992; Bache et al. 1999; Knowles and Hunt 2002; Li et al. 2015; Cruchley et al. 2015a, b, 2016; Németh et al. 2016, 2017; Hörnqvist et al. 2014; Viskari et al. 2013; Pineau and Antolovich 2009). Crack growth is then enhanced through fracture of the oxide intrusion (McMahon and Coffin 1970; Andrieu et al. 1992; Cruchley et al. 2015a, b; Németh et al. 2016, 2017). The oxide materials of which the intrusion is composed are brittle in comparison to the $\gamma$-matrix, with fracture toughnesses typically between 0.4 and 2 MPa m$^{1/2}$ (Evans 1995).

The stress field of a loaded intergranular crack has been widely assumed to enhance diffusion of oxygen along the grain boundary. This mechanism of failure of Ni-based superalloys at high temperatures has been called stress assisted grain boundary oxidation (SAGBO). It is quite different from the mechanism of Krupp (2005), which assumes the ingress of atomic oxygen weakens bonds at the grain boundary, resulting in decohesion. Németh et al. (2017) studied the temperature dependence of the ductility of a Ni-based superalloy in air between room temperature and 1000 °C. They observed a pronounced minimum in the ductility at 750 °C resulting from oxidation along the $\gamma$ grain boundaries and incoherent interfaces of $\gamma'$ particles. This experimental study, together with the experimental work of Kitaguchi et al. (2013), provide compelling evidence that the embrittlement is a result of the formation of oxide particles at grain boundaries rather than grain boundary decohesion due to the ingress of atomic oxygen. In this paper we assume the SAGBO mechanism of failure applies to Ni-based superalloys.

As might be expected in a multi-component superalloy the oxide intrusion is a complex agglomerate of nano-scale crystals in a layered structure (Kitaguchi et al. 2013), reflecting the decreasing chemical potential of oxygen with increasing distance normal to the grain boundary. The middle of the intrusion comprises fast growing oxides such as NiO and CoO, while the more thermodynamically stable oxides such as $Cr_2O_3$ and $Al_2O_3$, which can form at lower oxygen chemical

potentials, form in the outer layers of the intrusion. The intrusion is wedge-shaped. It is some tens of nanometres thick adjacent to the crack tip, and it tapers along the grain boundary over a distance of a few microns (McMahon and Coffin 1970; Andrieu et al. 1992; Li et al. 2015; Németh et al. 2016, 2017; Viskari et al. 2013; Kitaguchi et al. 2013, 2015). The length of the intrusion is much less than the length of the crack which is hundreds of microns (Andrieu et al. 1992; Viskari et al. 2013; Németh et al. 2017). In the matrix surrounding the intrusion and crack, slip bands have been observed (Németh et al. 2016; Hörnqvist et al. 2014), indicating that the failure is not purely brittle.

Karabela et al. (2013) simulated using finite elements, fatigue crack growth and oxygen diffusion in the Ni-based superalloy RR1000. They treated the grain microstructure explicitly and adopted a power law relationship for the inelastic strain rate. The diffusion of oxygen was assumed to be primarily along grain boundaries and assisted by stresses calculated using a crystal plasticity finite element model. They optimised the parameters of the simulation using experimental data for RR1000. They then obtained a fatigue failure curve for crack growth depending on both the oxygen concentration and accumulated inelastic strain at the crack tip, which compared well with experimental results. In contrast, the approach we have taken in this paper is theoretical, providing physical insight into the influence of the oxide intrusion on the fracture of the elastic–plastic medium through explicit functional relationships.

Evans et al. (2013) argued that diffusion of oxygen along the grain boundary is enhanced principally by creating a difference in the chemical potential of oxygen vacancies between the *ends* of the intrusion, and that the gradient of stress *within* the intrusion has a negligible effect. But to estimate the enhanced diffusion they assumed the variation of the normal stress within the intrusion ahead of the crack. In this paper we find the assumed variation in Evans et al. (2013) differs significantly from the profile we derive, most notably we find the intrusion adjacent to the crack tip is always loaded in tension for experimentally observed intrusion geometries. In addition, we find the gradient of the hydrostatic stress within the intrusion is consistent with experimental observations (Kitaguchi et al. 2013) of the growth of oxide intrusions under different loading conditions.

Chan (2014) argued that an oxide intrusion, with a larger volume per Ni atom than the Ni-matrix, induces a *compressive* stress in the matrix and thus screens the

crack tip. We find the opposite. In addition, Chan's use of the superposition principle of linear elasticity does not satisfy the boundary condition that the crack faces are free of tractions. In this paper we use the superposition principle in a self-consistent approach that satisfies the boundary conditions on the stress field.

The outline of the paper is as follows. In the next section we describe the geometry of the mathematical model, which includes a long crack, a misfitting intrusion at the crack tip, and a plastic zone ahead of the intrusion tip. In Sect. 3 we calculate the stress field of the isolated misfitting intrusion with a triangular cross-section in an infinite elastic medium with no applied stress. The superposition principle is used in Sect. 4 to add the stress field of the intrusion to the applied normal stress on the long crack. This is done by replacing the long crack by a semi-infinite crack and setting up an integral equation for the Burgers vector density of dislocations representing the crack and the plastic zone. The condition for the normal stress to be bounded at either end of the plastic zone enables the size of the plastic zone to be determined. This condition leads to the solution of the integral equation for the Burgers vector density, from which the crack tip opening displacement, the stress field, the local stress intensity factor at the crack tip, and the associated J-integrals are determined. A dimensionless parameter, which we call $\omega$, emerges from the analysis. It shows how the applied normal stress, the yield stress, the crack length, and the length of the intrusion conspire to control the influence of the intrusion on the embrittlement of the medium.

## 2 The geometry of the model

We consider an infinite, homogeneous, isotropic linear elastic medium in which there is a stationary crack of length $c$ in the plane $y = 0$, between $x = -c$ and $x = 0$, and which is infinitely extended along the $z$-axis. There is a uniform applied stress $\sigma_{yy} = \sigma$ at $y = \pm\infty$. The stress intensity factor of the crack is $K_I = \sigma\sqrt{\pi c}$. Ahead of the crack there is a grain boundary occupying the half-plane $y = 0$, $x \geq 0$. We assume there is an oxide intrusion at the crack tip with a triangular cross-section, and infinitely long along the $z$-axis, as shown in Fig. 1. The base of the intrusion is at the crack-tip and has width t, and its tip is at $x = l \geq 0$. We assume a plastic zone between $x = l$ and $x = a > l$, and infinitely extended along the $z$-axis, in which the stress
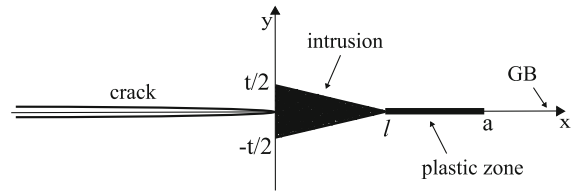


**Fig. 1** Geometry of the model comprising a long stationary crack along the negative $x$-axis, an intrusion with a triangular cross-section and a plastic zone. The model is subjected to an applied stress $\sigma_{yy} = \sigma$ at $y = \pm\infty$, so the crack is loaded in mode I. The geometry is invariant normal to the page and therefore the elastic field is one of plane strain

is constant and equal to the yield stress, $\sigma_1$. In line with experimental observations we assume the crack is much longer than the intrusion, $c \gg l$. This is a plane strain model because the strain tensor has non-zero components $e_{xx}$, $e_{yy}$, $e_{xy}$ only. As the length $l$ of the intrusion tends to zero the plastic zone approaches the crack tip and the model becomes equivalent to the DBCS-model (Dugdale 1960; Bilby et al. 1963) with a long crack. As the angle at the tip of the intrusion tends to zero the intrusion vanishes and it is replaced by a dislocation-free zone (DFZ) occupying the region $0 \leq x \leq l$. We call this limit the DFZ-model (Chang and Ohr 1981, 1983; Ohr and Chang 1982; Majumdar and Burns 1983; Weertman et al. 1983). These models are instructive limiting cases for comparison to our model.

## 3 The intrusion

In this section we calculate the stress field in an infinite medium arising from the intrusion only with no applied stress.

### 3.1 The stress tensor

For simplicity we assume the elastic constants of the intrusion are those of the surrounding isotropic elastic medium. The intrusion is assumed to be homogeneous and to be characterised only by its volumetric misfit. Assuming the intrusion is composed of NiO the volumetric misfit is $\Phi = 1.65$ (Evans 1995). That is, when the intrusion forms its stress-free volume is 1.65 times greater than the volume occupied by the same number of nickel atoms in the superalloy. Assuming the dilatation is isotropic the linear misfit strain is then $\epsilon_m = \sqrt[3]{\Phi} - 1 = 0.18$.

Let the interface between the intrusion and the matrix be labelled $\Gamma$. We associate with $\Gamma$ a contin-
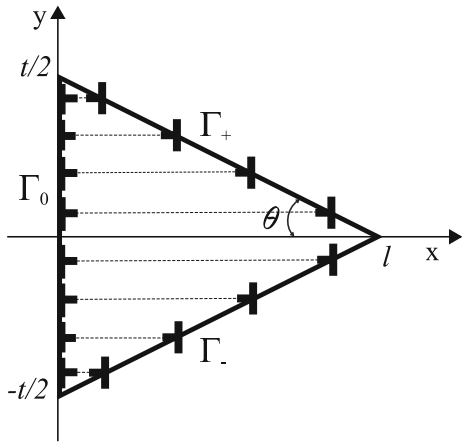
**Fig. 2** Schematic illustration of a cross-section of the intrusion. The intrusion semi-angle $\theta$ is enlarged for clarity. The 18% misfit along $y$ is represented by a continuous distribution of interfacial edge dislocations. It is assumed the same misfit along $x$ and $z$ cannot be sustained elastically because $l \gg t$ and the intrusion has infinite length along $z$, so that the misfit is assumed to be fully relaxed along $x$ and $z$. Note the extra half planes of the dislocations are inside the intrusion because it has a larger volume when it is stress-free. The dislocations form interstitial loops, closed at $z = \pm\infty$

uous distribution of dislocations, which generates the elastic field of the intrusion. In Fig. 2 the dimensions of the intrusion are those of a triangular prism of the Ni-matrix before it has been oxidised. The interface $\Gamma$ comprises a vertical interface, $\Gamma_0$, and two inclined interfaces $\Gamma_+$ and $\Gamma_-$ (see Fig. 2). The intrusion semi-angle is $\theta = \arctan[t/2l]$. TEM observations show that $\theta \ll 1$ (Kitaguchi et al. 2013). Since $t \ll l$ we assume the 18% misfit along $y$ is accommodated elastically. That is, the interface $\Gamma$ is in a state of forced elastic coherence along the $y$-axis. This is modelled by a continuous distribution of edge dislocations with infinitesimal Burgers vectors along the negative $y$-axis, and with their lines parallel to $z$, consistent with the FS/RH convention. But since the interface along the $z$-axis is infinitely long we assume it is fully incoherent along $z$, that is there are no dislocations with Burgers vectors along $z$. Similarly, since $l \gg t$ we assume the interfaces cannot sustain coherency along the $x$-direction and therefore these interfaces do not have dislocations with Burgers vectors parallel to $x$. Figure 2 shows schematically the continuous distribution of interfacial edge dislocations with Burgers vectors along $-y$ and infinitely long lines parallel to $z$ forming loops closed at $z = \pm\infty$. The elastic field of the intrusion is generated by this continuous distribution of dislocations.

To model the volumetric misfit of the intrusion we assign a positive sign to the line sense along $\Gamma_0$ and a negative sign to the line sense along $\Gamma_+$ and $\Gamma_-$. Let $\boldsymbol{\gamma}$ be the position vector of a point on the interface $\Gamma$, and $d\boldsymbol{\gamma}$ be an infinitesimal element of $\Gamma$. Let $b(\boldsymbol{\gamma})d\gamma$ be the magnitude of the Burgers vector of the continuously distributed dislocations between $\boldsymbol{\gamma}$ and $\boldsymbol{\gamma} + d\boldsymbol{\gamma}$. Then the Burgers vector density $b(\boldsymbol{\gamma})$ is as follows:

$$b(\boldsymbol{\gamma}) = \epsilon_{\mathrm{m}} \times \begin{cases} -1, & \text{if } \boldsymbol{\gamma} \in \Gamma_0 \\ \sin\theta, & \text{if } \boldsymbol{\gamma} \in \Gamma_{\pm}. \end{cases} \quad (1)$$

The total Burgers vector of the continuously distributed dislocations on $\Gamma$ vanishes:

$$0 = \oint_{\Gamma} d\gamma \, b(\boldsymbol{\gamma}). \quad (2)$$

The stress tensor for the intrusion, $\sigma_{\alpha\beta}^I(\mathbf{x})$, is then:

$$\sigma_{\alpha\beta}^I(\mathbf{x}) = \oint_{\Gamma} d\gamma \, \frac{\mu \, b(\boldsymbol{\gamma})}{2\pi(1-\nu)} \zeta_{\alpha\beta}(\mathbf{x} - \boldsymbol{\gamma}), \quad (3)$$

where $\mathbf{x} = (x, y)$ and $\mu$ and $\nu$ are the shear modulus and Poisson's ratio, and the functions $\zeta_{\alpha\beta}(\mathbf{x})$ are determined by the stress field of a positive edge dislocation:

$$\begin{aligned} \zeta_{xx}(\mathbf{x}) &= \frac{x(x^2 - y^2)}{(x^2 + y^2)^2}, \\ \zeta_{yy}(\mathbf{x}) &= \frac{x(3y^2 + x^2)}{(x^2 + y^2)^2}, \\ \zeta_{xy}(\mathbf{x}) &= \zeta_{yx}(\mathbf{x}) = \frac{y(x^2 - y^2)}{(x^2 + y^2)^2}, \\ \zeta_{zz}(\mathbf{x}) &= \nu \left( \zeta_{xx}(\mathbf{x}) + \zeta_{yy}(\mathbf{x}) \right), \\ \zeta_{xz}(\mathbf{x}) &= \zeta_{zx}(\mathbf{x}) = \zeta_{yz}(\mathbf{x}) = \zeta_{zy}(\mathbf{x}) = 0. \end{aligned} \quad (4)$$

It is convenient to introduce a stress $\sigma_0 = \mu\epsilon_{\mathrm{m}}/2\pi(1-\nu)$. In RR1000 the shear modulus and Poisson's ratio are $\mu = 74$ GPa and $\nu = 0.285$ (Karabela et al. 2013) at $650\,°\mathrm{C}$, for which $\sigma_0 = 2.96$ GPa. These elastic constants are used throughout the paper whenever stresses in RR1000 are calculated.

3.2 The hydrostatic stress along the $x$-axis

The hydrostatic stress is of interest because oxygen vacancies experience a force to drift from regions of hydrostatic tension to regions of hydrostatic compression. We obtain the following expression for the hydrostatic stress on the $x$-axis, $\sigma^I(x, 0) = \frac{1}{3} \sum_{\alpha} \sigma_{\alpha\alpha}^I(x, 0)$:
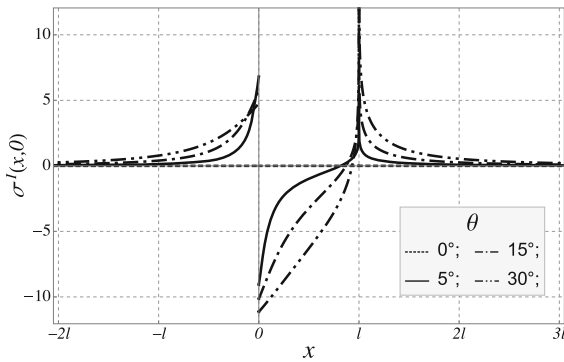
**Fig. 3** The hydrostatic stress $\sigma^I(x, 0)$ (5) in GPa generated by the intrusion along the $x$-axis for RR1000, plotted as a function of $x$ for four values of the intrusion semi-angle $\theta$

$$
\sigma^I(x, 0)
$$
$$
= -\frac{\sigma_0(1 + \nu)}{3}\left[2(\cos(2\theta) + 1)\arctan\left(\frac{l\tan\theta}{x}\right)\right.
$$
$$
+ \sin(2\theta)\log\left(\frac{(x - l)^2}{x^2 + l^2\tan^2\theta}\right)
$$
$$
\left. + 2\pi(1 - \cos(2\theta))\left(H(x) - H(x - l)\right)\right], \quad (5)
$$

where $H(x)$ denotes the Heaviside step function. We note that as $\theta \to 0$, $\sigma^I(x, 0) \to 0$, as it should because in this limit the intrusion vanishes. But when $\theta > 0$, the hydrostatic stress is discontinuous at $x = 0$. The discontinuity does not depend on the intrusion angle throughout the range $0 < \theta \le \pi/2$:

$$
\lim_{\delta \to 0} \ \sigma^I(-\delta, 0) - \sigma^I(\delta, 0) = \frac{4\pi}{3}(1 + \nu)\sigma_0. \quad (6)
$$

The jump in the hydrostatic stress at $x = 0$ is 15.9 GPa for RR1000.

The hydrostatic stress along the $x$-axis is plotted in Fig. 3 for RR1000 as an illustration of (5). The hydrostatic stress is tensile on the $x$-axis at all intrusion angles just outside the intrusion and compressive just inside at $x = 0$. As expected the thickest part of the intrusion is always in compression. At the apex of the intrusion the hydrostatic stress is always tensile both inside and outside the intrusion, diverging logarithmically as the tip is approached from both sides along the $x$-axis.
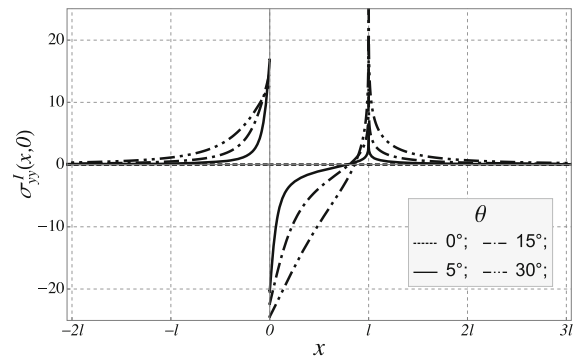


**Fig. 4** The normal stress $\sigma_{yy}^I(x, 0)$ (7) in GPa generated by the intrusion along the $x$-axis for RR1000, plotted as a function of $x$ for four values of the intrusion semi-angle $\theta$

### 3.3 The normal stress along the $x$-axis

The normal stress $\sigma_{yy}^I(x, 0)$ is of interest because it will contribute to tractions on the crack faces in the next section. We obtain the following expression for it:

$$
\sigma_{yy}^I(x, 0) = \sigma_0\left[l\sin(2\theta)\frac{x - l\tan^2\theta}{x^2 + l^2\tan^2\theta}\right.
$$
$$
- 4\pi\sin^4\theta\left(H(x) - H(x - l)\right)
$$
$$
+ \left(\frac{\cos(4\theta)}{2} - 2\cos(2\theta) - \frac{5}{2}\right)\arctan\left(\frac{l\tan\theta}{x}\right)
$$
$$
\left. + \left(\frac{\sin(4\theta)}{4} - \sin(2\theta)\right)\log\left(\frac{(x - l)^2}{x^2 + l^2\tan^2\theta}\right)\right].
$$
$$
(7)
$$

This function is plotted in Fig. 4 for RR1000. The normal stress is predominantly compressive inside the intrusion, becoming more so as the intrusion angle increases. The normal stress becomes tensile inside the intrusion near the tip at $x = l$, and $\sigma_{yy}^I(x, 0)$ diverges as $-\sin(2\theta)(1 + 2\sin^2\theta)\log|x - l|$ as $x \to l$. This is a geometrical effect arising from the tapered shape of the intrusion. Outside the intrusion $\sigma_{yy}^I(x, 0)$ is everywhere tensile and it becomes negligible at distances of more than two intrusion lengths from the intrusion.

## 4 The intrusion at the crack tip

In this section we use the stress field of the intrusion to calculate the stress field and related properties of the whole model portrayed in Fig. 1.

## 4.1 The approximation of a semi-infinite crack

The crack and the plastic zone are modelled as continuous distributions of climb edge dislocations in the usual way, e.g. Lardner (1974). These dislocations have infinitesimal Burgers vectors along the negative $y$-axis and lines parallel to the $z$-axis, consistent with the FS/RH convention. The total traction at any point on the faces of the crack must be zero. The sources of the traction are the stress fields of the dislocations comprising the crack, the applied load $\sigma$, and the stresses created by the intrusion and dislocations in the plastic zone. The $xy$-component of the total stress tensor on the crack faces is zero by virtue of the mirror symmetry in the plane $y = 0$. The $yz$-component of the total stress tensor on the crack faces is zero because the strain field is confined to the $x - y$ plane. Therefore, only the $yy$ component of the total stress tensor on the crack faces has to be considered. For the plastic zone we assume the $yy$-component of the total stress tensor is a constant, $\sigma_1$, which we interpret as the yield stress. Let $L_c$ denote the set of points along the $x$-axis occupied by the crack, $-c \leq x \leq 0$, and the plastic zone $l \leq x \leq a$, where $c \gg l, a$. In $L_c$ the Burgers vector density of the dislocations is $b_c(x)$. Then, at any point $x$ in the crack or plastic zone we require the following singular integral equation to be satisfied:

$$A \int_{L_c} dx' \frac{b_c(x')}{x - x'} = \sigma_1 \left( H(x - l) - H(x - a) \right)$$
$$- \sigma_{yy}^I(x, 0) - \sigma, \qquad (8)$$

where $A = \mu/2\pi(1 - \nu)$. The integral is a Cauchy principal value integral because a straight dislocation does not exert a stress upon itself. The term involving two Heaviside step functions is equal to $\sigma_1$ if $x$ is in the plastic zone, otherwise it is zero. In this equation the addition of the intrusion stress tensor, $\sigma_{yy}^I$, to the applied load $\sigma$ is an application of the superposition principle.

In (8) we see that the integral extends over the entire crack length, $c$, and the plastic zone. But provided $c$ is much larger than the intrusion and the plastic zone it is otherwise arbitrary. This dependence on $c$ complicates the analysis unnecessarily and it may be removed, as we now show.

We have already noted in Fig. 4 that the stress $\sigma_{yy}^I(x, 0)$ generated by the intrusion is negligible at distances along the $x$-axis from the intrusion of more

than twice its length. In small-scale yielding the field of the plastic zone is also short ranged compared to the crack length. Therefore, the intrusion and plastic zone modify the distribution of Burgers vectors in the crack only in the vicinity of its tip at $x = 0$. Conversely, the intrusion and plastic zone are in the near-tip stress field of the crack. Summarising, the Burgers vector density inside the crack is modified by the intrusion and plastic zone near the tip at $x = 0$ only, and the intrusion and plastic zone are located in the stress field $\sigma_{yy}(x, 0)$ of the crack only slightly ahead of this tip.

Since most of the crack surfaces are unaffected by the presence of the intrusion and plastic zone, we may view their presence as a perturbation localised near the crack tip. However, we will see below that they affect the stress intensity factor of the crack significantly. Let $b_e(x)$ be the Burgers vector density of an elastic crack of length $2c$, occupying $-2c \leq x \leq 0$ and $y = 0$, in an infinite elastic medium. The crack is subjected to an applied normal load $\sigma$ at $y = \pm\infty$, and the intrusion and plastic zone are absent. Our crack of length $c$ will be modelled as half of this crack of length $2c$, occupying $-c \leq x \leq 0$. We view $b_e(x)$ as an unperturbed Burgers vector density of an elastic crack because it is not disturbed by the plastic zone or intrusion. It is well known, e.g. Lardner (1974), that $b_e(x)$ is as follows:

$$b_e(x) = \frac{\sigma}{A\pi} \frac{(x + c)}{\sqrt{-x(2c + x)}}. \qquad (9)$$

This distribution ensures the crack faces are free of tractions along their entire length. Ahead of the crack, at $x > 0$, we obtain the stress $\sigma_{yy}^e(x, 0)$:

$$\sigma_{yy}^e(x, 0) = \sigma + A \int_{-2c}^{0} dx' \frac{b_e(x')}{x - x'} = \sigma \frac{(x + c)}{\sqrt{x(2c + x)}}$$
$$= \frac{K_I}{\sqrt{2\pi x}} + O\left(\frac{x}{c}\right). \qquad (10)$$

The same stress field $\sigma_{yy}^e(x, 0)$ just ahead of the crack may be obtained by extending the crack to $x = -\infty$, so that it occupies $-\infty \leq x \leq 0$, and by introducing the following Burgers vector density into the semi-infinite crack:

$$b_e^{(0)}(x) = \frac{K_I}{A\pi \sqrt{-2\pi x}}, \qquad (11)$$

where $K_I$ is the same stress intensity $\sigma\sqrt{\pi c}$. By comparing with (9) it is seen that $b_e(x) = b_e^{(0)}(x) + O(x/c)$. Therefore it is a good approximation to replace the

unperturbed Burgers vector density $b_e(x)$ with $b_e^{(0)}(x)$ to model (a) the stress field just ahead of the crack tip at $x = 0$ and (b) the Burgers vector density just inside the crack near $x = 0$. However, the traction on the crack faces within the semi-infinite crack with the Burgers vector density $b_e^{(0)}(x)$ is then zero, not $-\sigma$ as it should be. It follows that if we replace $b_e(x)$ in the finite crack of length $2c$ in (8) with $b_e^{(0)}(x)$ in a semi-infinite crack we must remove the applied stress $\sigma$ from the right hand side of the equation. Equation (8) then becomes:

$$A \int_L dx' \frac{b(x')}{x - x'} = \sigma_1 \left( H(x - l) - H(x - a) \right)$$

$$-\sigma_{yy}^I(x, 0) \equiv P(x), \qquad (12)$$

where $L$ extends from $x' = -\infty$ to $x' = 0$ and from $x' = l$ to $x' = a$, and $b(x)$ is the Burgers vector density of the dislocations in $L$. Thus, the removal of the dependence on the crack length $c$ from the equilibrium condition in (8) has been achieved without compromising the accuracy of the model in the crucial region near the crack tip. Attention can now be focused on the Burgers vector density $b(x)$ in this region, where the interaction with the intrusion and plastic zone dominate.

### 4.2 The solution of the integral equation

To solve the integral equation (12) we introduce the complex function $g(z) = i\sqrt{z/[(z - l)(z - a)]}$, where $z = x + iy$. Then, using the techniques described by Lardner (1974) the formal solution is as follows:

$$b(x) = \frac{1}{A\pi^2 g(x + i0)} \int_L dx' \frac{g(x' + i0)P(x')}{x' - x}. \quad (13)$$

This solution exists when the following condition is satisfied:

$$K_I \sqrt{\frac{\pi}{2}} = \int_L dx' \, g(x' + i0) P(x'). \qquad (14)$$

This condition ensures the Burgers vector density is finite at the ends $x = l$ and $x = a$ of the plastic zone, as required by the finite value of $\sigma_1$ throughout the plastic zone.

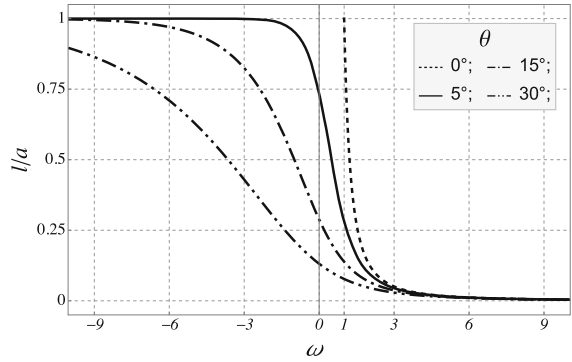The condition in (14) provides a relationship for the size of the plastic zone. Let $\eta = l/a$. The plastic zone



**Fig. 5** Graphical representation of (15) for $\eta = l/a$ as a function of $\omega$ for four values of the intrusion semi-angle $\theta$. When $\eta = 1$ there is no plastic zone and as $\eta \to 0$ the plastic zone becomes infinitely long. In particular when $\theta = 0$ the plastic zone vanishes at $\omega = 1$ and there are no solutions for $\omega < 1$

has length $a - l = l(1 - \eta)/\eta$. The evaluation of the integral in (14) provides the following implicit relationship for $\eta$ in terms of the dimensionless variable $(\sigma/\sigma_1)\sqrt{c/(2l)}$:

$$\frac{\sigma}{\sigma_1}\sqrt{\frac{c}{2l}} = \frac{2}{\pi} \frac{\mathrm{E}(1 - \eta)}{\sqrt{\eta}} - \frac{\sigma_0}{\sigma_1} \sqrt{\eta} \left( \frac{2\sin^{3/2}\theta \cos\chi}{\sqrt[4]{1 + \eta^2 \tan^2\theta}} \right.$$
$$\left. + \Re\mathrm{e}\left[ \left( e^{i4\theta} - 4e^{i2\theta} - 5 \right) \Pi\left(1 - \eta; \phi | 1 - \eta\right) \right] \right). \qquad (15)$$

In this equation $\chi = 3\theta/2 + \pi/4 + \arctan[\eta \tan\theta]/2$, and $\mathrm{E}(m)$ and $\Pi(n; \phi|m)$ are respectively the complete elliptic integral of the second kind and the incomplete elliptic integral of the third kind, where $m$ is the parameter, $n$ is the characteristic, and the amplitude $\phi = \arctan\left[\sqrt{(i \tan\theta - 1)/(1 - i \eta \tan\theta)}\right]$. There is ambiguity in the definitions of the elliptic integrals in the literature. In the Appendix we state the definitions used in this paper for the incomplete and complete elliptic integral of the first, second and third kinds. Here and elsewhere in this paper we assume $\sigma_0/\sigma_1 = 3$ as in RR1000 at 650 °C. The variable $\omega \equiv (\sigma/\sigma_1)\sqrt{c/(2l)}$ is a ratio of stress intensity factors, combining the applied stress $\sigma$, the yield stress $\sigma_1$, the crack length $c$ and the length of the intrusion $l$ into a single dimensionless variable. *We will show that the conditions under which the intrusion embrittles the material are described by a limited range of values of $\omega$.*

The solution of (15) for $\eta$ is plotted in Fig. 5 for four values of the intrusion semi-angle. When $\theta = 0$ there is no intrusion. The presence of the intrusion increases

the size of the plastic zone. As $\theta$ increases the size of the plastic zone increases for a given value of $\omega$. We note that even when the applied stress is compressive (so that $\omega < 0$) there is still a plastic zone ahead of the intrusion. All these features stem from the tensile normal stress ahead of the intrusion seen in Fig. 4, which increases with $\theta$.

Using (15) the solution of (13) for the Burgers vector density $b(x)$ becomes:

$$b(x) = \frac{1}{A\pi} \eta \, j(x + i0) \left[ \frac{2\sigma_1}{\pi} \Pi \left( \frac{(1-\eta)x}{x-l} \bigg| 1-\eta \right) \right.$$
$$- \sigma_0 \left( \frac{2 \sin^{3/2}\theta \cos\chi}{\sqrt[4]{1 + \eta^2 \tan^2\theta}} \frac{(l-x)(l\tan\theta\tan\chi - x)}{x^2 + l^2 \tan^2\theta} \right.$$
$$+ \Re e \left[ \left( e^{i4\theta} - 4e^{i2\theta} \right.\right.$$
$$\left.\left.\left. -5 \right) \Pi \left( \frac{(1-\eta)x}{x-l}; \phi \bigg| 1-\eta \right) \right] \right) \right]. \qquad (16)$$

In this expression we follow the convention (Abramowitz and Stegun 1972) that whenever the phase of the elliptic integral of the third kind is not specified—as in the first occurrence of $\Pi$ on the right hand side of this equation—it is understood the phase is $\pi/2$ and the integral is then a *complete* elliptic integral of the third kind. Also, $j(z) = i\sqrt{[a(z-a)]/[z(z-l)]}$.

### 4.3 The crack tip opening displacement

We may use Eq. (16) for the Burgers vector density to calculate the crack tip opening displacement as follows:

$$\Delta u = \int_l^a dx \, b(x)$$
$$= \frac{a}{A\pi} \left\{ \frac{2\sigma_1}{\pi} \left[ (E(1-\eta))^2 - \eta(K(1-\eta))^2 \right] \right.$$
$$+ \sigma_0 \left[ \frac{4\eta \sin^{3/2}\theta \cos\chi}{\sqrt[4]{1 + \eta^2 \tan^2\theta}} \left[ \frac{\tan\chi}{\tan\theta} K(1-\eta) - E(1-\eta) \right] \right.$$
$$+ \Re e \left[ \left( e^{i4\theta} - 4e^{i2\theta} - 5 \right) \left( K(1-\eta) \, Z(\phi|1-\eta) \right.\right.$$
$$+ \eta K(1-\eta) \, F(\phi|1-\eta) - E(1-\eta) \, E(\phi|1-\eta)$$
$$+ \frac{i\pi}{2}(1-\eta)$$
$$\left. + \sqrt{\frac{(1 - i\eta\tan\theta)(i\tan\theta - 1)}{i\tan\theta}} E(1-\eta) \right)$$
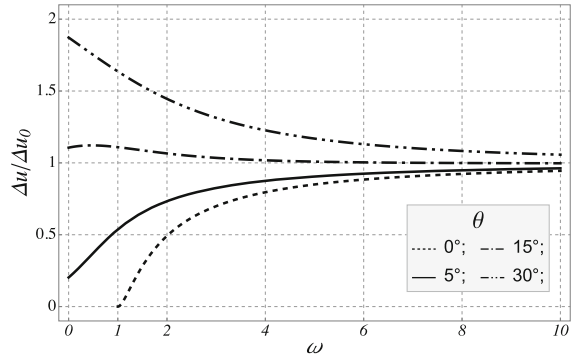




**Fig. 6** The crack tip opening displacement $\Delta u$, normalised to the crack tip opening displacement of the DBCS-model model $\Delta u_0$, plotted as a function of $\omega$ for four values of the intrusion semi-angle $\theta$

$$+ \left( \frac{4i \, \eta \sin^{1/2}\theta \cos\theta \, e^{i\chi}}{\sqrt[4]{1 + \eta^2 \tan^2\theta}} \right.$$
$$+ \left( e^{i4\theta} - 4e^{i2\theta} - 5 \right) \sqrt{\frac{1 - i\eta\tan\theta}{i\tan\theta(i\tan\theta - 1)}} \right)$$
$$\left.\left.\left.\left. \times (1 - i\eta\tan\theta)\Pi \left( \frac{(1-\eta)\tan\theta}{\tan\theta + i} \bigg| 1-\eta \right) \right] \right] \right\}. \quad (17)$$

In this expression $Z(\phi|m)$ is the Jacobi Zeta function, $K(m)$ is the complete elliptic integral of the first kind, and $F(\phi|m)$ and $E(\phi|m)$ are the incomplete elliptic integrals of the first and second kind, respectively. This expression for $\Delta u$ is plotted in Fig. 6, where it is normalised to the crack tip opening displacement $\Delta u_0 = 2a\sigma_1/(A\pi^2)$ in the DBCS-model. The length of the plastic zone is $a \ll c$. When $\theta = 0$, taking the limit as $l \to 0$, we recover the DBCS-model and the crack tip opening displacement approaches $\Delta u_0$. But in the presence of an intrusion (i.e. $\theta > 0$), the crack tip opening displacement increases with $\theta$ at a given value of $\omega$. This is consistent with Fig. 5 where the size of the plastic zone increases with $\theta$ for a given value of $\omega$. The asymptotic behaviour of all the curves in Fig. 6 at large values of $\omega$ reflects the diminishing significance of the intrusion as the intrusion length $l$ decreases relative to the crack length $c$, and as the applied stress $\sigma$ increases relative to the yield stress $\sigma_1$.

### 4.4 The normal stress along the $x$-axis

The stress field in the medium is generated by edge dislocations with density $b(x)$ (16) in the crack and

plastic zone, and by the intrusion. The total stress tensor, $\sigma_{\alpha\beta}(\mathbf{x})$, is given by the superposition principle of linear elasticity:

$$
\sigma_{\alpha\beta}(\mathbf{x}) = \int\limits_L dx' \, A \, b(x') \, \zeta_{\alpha\beta}\left(x - x', y\right)
$$
$$
+ \sigma_{\alpha\beta}^I(\mathbf{x}). \tag{18}
$$

The functions $\zeta_{\alpha\beta}(\mathbf{x})$ are defined in (4). The integrals in (18) may be evaluated by complex variable techniques, and the resulting components of the total stress tensor are stated in the Supplementary Material. The normal stress $\sigma_{yy}(x, 0)$ is of interest because it governs the fracture of the grain boundary and, hence, of the intrusion. In the crack this normal stress is zero, in the plastic zone it is $\sigma_1$, and at other positions along the $x$-axis it is as follows:

$$
\sigma_{yy}(x, 0)
$$
$$
= \eta \sqrt{\frac{a(a - x)}{x(l - x)}} \left[ \frac{2\sigma_1}{\pi} \Pi\left( \frac{(1 - \eta)x}{x - l} \middle| 1 - \eta \right) \right.
$$
$$
+ \sigma_0 \left( \frac{2\sin^{3/2}\theta \cos\chi}{\sqrt[4]{1 + \eta^2 \tan^2\theta}} \frac{(x - l)(l\tan\theta\tan\chi - x)}{x^2 + l^2\tan^2\theta} \right.
$$
$$
\left. \left. + \Re\left[ \left(5 + 4e^{i2\theta} - e^{i4\theta}\right) \Pi\left( \frac{(1 - \eta)x}{x - l}; \phi \middle| 1 - \eta \right) \right] \right) \right]
$$
$$
- 4\pi\sigma_0 \left( H(x) - H(x - l) \right). \tag{19}
$$

In Fig. 7 we plot $\sigma_{yy}(x, 0)$ for an intrusion with a semi-angle $\theta = 5°$, for four values of $\omega$ from $-1$ to 40. It is seen that the normal stress at the tip of the intrusion approaches $\sigma_1$ for all values of $\omega$ and this small value of $\theta$. This is also obtained in (19):

$$
\lim_{x \to l^-} \sigma_{yy}(x, 0) = \sigma_1 + \frac{\pi\sigma_0}{2} \left( 4\cos(2\theta) - \cos(4\theta) - 3 \right)
$$
$$
= \sigma_1 - 4\pi\sigma_0 \theta^4 + O\left(\theta^6\right). \tag{20}
$$

This equation shows that for experimentally observed intrusion geometries the normal stress at the intrusion tip is finite and equal to $\sigma_1$. In contrast, at the crack tip there is always a tensile square root singularity.

It is interesting to compare the solid curve in Fig. 7, showing $\sigma_{yy}(x, 0)$ when there is no applied stress ($\omega = 0$), with the curve in Fig. 4 for $\theta = 5°$, showing the stress generated by the intrusion only. The presence of the crack tip singularity in Fig. 7, and its absence in Fig. 4, puts *both* ends of the intrusion into normal tension in Fig. 7, although at the thicker end of the intru-
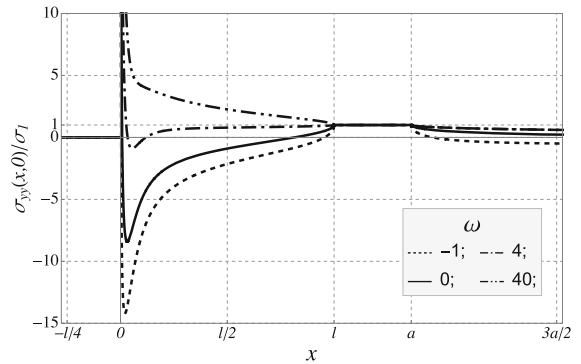


**Fig. 7** The $yy$-component of the total stress tensor on the $x$-axis for RR1000 as a function of $x$ for four values of $\omega$ from $-1$ to 40. The intrusion semi-angle, $\theta$, is constant and equal to $5°$. The normal stress $\sigma_{yy}(x, 0) = 0$ in the crack, for which $x \le 0$. The intrusion lies between $x = 0$ and $x = l$. In the plastic zone $\sigma_{yy}(x, 0) = \sigma_1$ and it is between $x = l$ and $x = a$. Note that $a$ varies with $\omega$
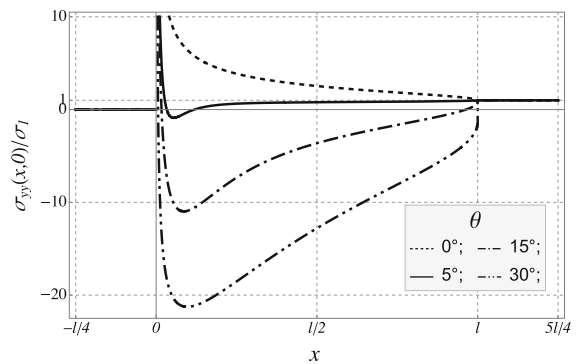


**Fig. 8** The $yy$-component of the stress tensor plotted against $x$ for RR1000 for four values of the intrusion angle $\theta$, and $\omega = 4$

sion ($x = 0^+$) the tensile region is very narrow at the smallest values of $\omega$. This feature persists even when the applied load is slightly compressive ($\omega = -1$).

It is seen that as $\omega$ increases the spatial extent of the compressive region inside the intrusion diminishes and eventually all the intrusion is in normal tension. This behaviour changes the gradient of $\sigma_{yy}(x, 0)$ inside the intrusion significantly—a point we return to in Sect. 5.

In Fig. 8 we show the normal stress $\sigma_{yy}(x, 0)$ when $\omega = 4$ for four values of intrusion semi-angle $\theta$. As the intrusion semi-angle decreases the normal stress $\sigma_{yy}(x, 0)$ inside the intrusion becomes increasingly tensile; when $\theta = 5°$ there is only a very small part of the $x$-axis where the normal stress is compressive.
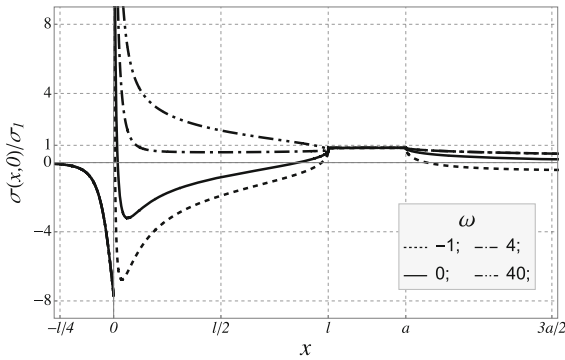
**Fig. 9** The hydrostatic stress on the $x$-axis for RR1000 as a function of $x$ for four values of $\omega$ from $-1$ to $40$. The intrusion semi-angle, $\theta$, is constant and equal to $5°$. The hydrostatic stress $\sigma(x, 0) < 0$ in the crack, for which $x \leq 0$. The intrusion lies between $x = 0$ and $x = l$. In the plastic zone $\sigma(x, 0) \approx \sigma_1$ and it is between $x = l$ and $x = a$

### 4.5 The hydrostatic stress along the $x$-axis

We obtain the following expression for the hydrostatic stress on the $x$-axis, $\sigma(x, 0) = \frac{1}{3} \sum_\alpha \sigma_{\alpha\alpha}(x, 0)$:

$$\sigma(x, 0) = \frac{2(1 + \nu)}{3} \left( \sigma_{yy}(x, 0) - \sigma_{yy}^I(x, 0) \right) + \sigma^I(x, 0). \tag{21}$$

In Fig. 9 we plot $\sigma(x, 0)$ for an intrusion with a semi-angle $\theta = 5°$, for four values of $\omega$ from $-1$ to $40$. It is seen that the hydrostatic stress is similar to the normal stress illustrated in Fig. 7. However, the crack faces are under compression and the compressive stress inside the intrusion is smaller than that in Fig. 7.

### 4.6 The local stress intensity factor

Let $k_I$ be the local stress intensity factor of the crack tip. It is defined by $k_I = \lim_{x \to 0^+} \sqrt{2\pi x} \, \sigma_{yy}(x, 0)$. It differs from the applied stress intensity factor $K_I$ owing to the interaction with the intrusion and the plastic zone. Using (19) we obtain the following expression for $k_I$:

$$k_I = \sqrt{2\pi l} \left[ \frac{2\sigma_1}{\pi} \mathrm{K}(1 - \eta) - \sigma_0 \left( \frac{2 \sin^{1/2} \theta \cos \theta \sin \chi}{\sqrt[4]{1 + \eta^2 \tan^2 \theta}} \right. \right.$$
$$\left. \left. + \Re e \left[ \left( 5 + 4e^{i2\theta} - e^{i4\theta} \right) \mathrm{F}(\phi | 1 - \eta) \right] \right) \right]. \tag{22}$$

In Fig. 10 we plot $k_I/K_I$ as a function of $\omega$ for four values of the intrusion semi-angle $\theta$. Taking the limit $l \to 0$ in (22) we obtain $k_I = 0$ because the model
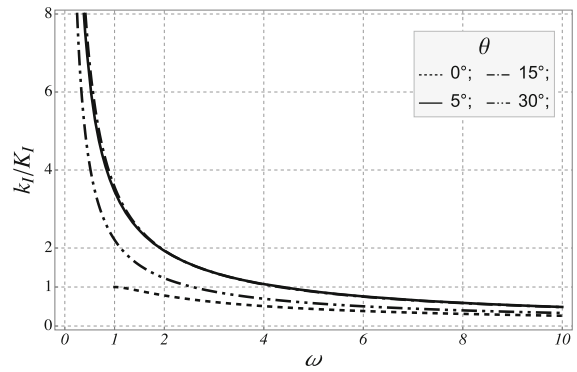


**Fig. 10** Plot of the local stress intensity factor, $k_I$, normalised to $K_I$, as a function of $\omega$ for four values of the intrusion semi-angle

then becomes equivalent to the DBCS-model where the crack tip is completely screened by the plastic zone. This is also evident in Fig. 10 where $k_I/K_I \to 0$ as $\omega \to \infty$.

It is seen in Fig. 10 that when $\theta > 0$ the presence of the intrusion raises $k_I$ above the local stress intensity factor of the DFZ-model. This shows that the existence of the intrusion, as compared with its replacement by a DFZ of the same length, increases the intensity of the stress singularity at the crack tip. $k_I$ increases with the length $l$ of the intrusion. The size of the plastic zone increases with increasing $\omega$, as seen in Fig. 5, which increasingly screens and blunts the crack tip. A more ductile material, characterised by a smaller value of the yield stress $\sigma_1$, or a larger applied stress $\sigma$, reduces the stress intensification at the crack tip caused by the intrusion. When $\theta = 30°$ the larger plastic zone screens the crack more effectively and $k_I$ is lower than that for $\theta = 5°$ and $15°$, as seen in Fig. 10.

### 4.7 J-integrals

Eshelby (1951, 1956) derived the force on an elastic singularity as an integral taken around a contour enclosing the singularity, a result that was discovered independently by Rice (1968) who called it the J-integral. We consider three contours, $S_1$, $S_2$ and $S_3$, illustrated in Fig. 11. The radius of $S_1$ is very large compared to the crack tip, intrusion and plastic zone which it encloses. $S_2$ is a contour around the crack tip only with an infinitesimal radius. $S_3$ encloses the plastic zone only. The non-zero component, $J_x$, of the J-integral for each of these contours is then:
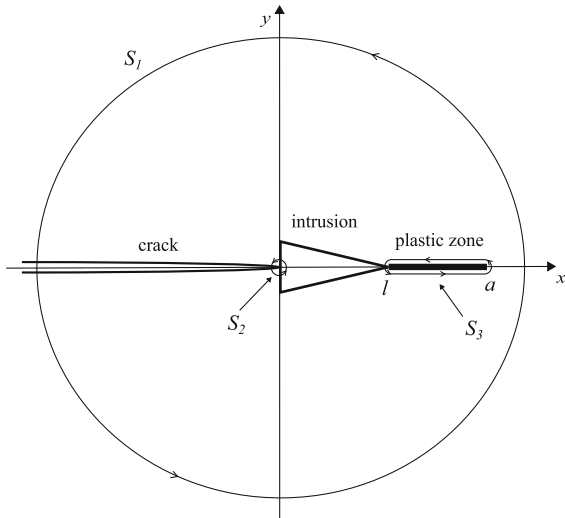
**Fig. 11** The contours $S_1$, $S_2$ and $S_3$ comprise the singularities of the medium (i.e. the crack tip and the plastic zone)
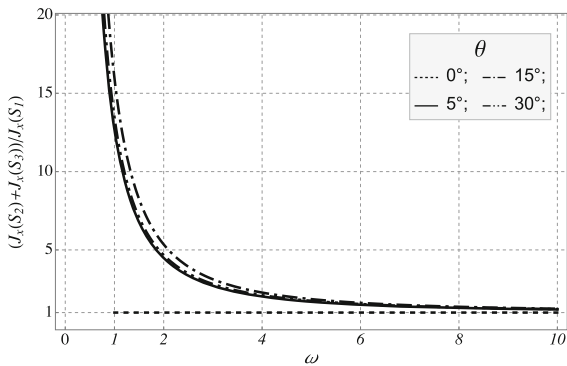


**Fig. 12** The ratio of $J_x(S_2) + J_x(S_3)$ to $J_x(S_1)$, given by (23) as a function of $\omega$ for four values of the intrusion semi-angle $\theta$, and $\sigma_0 = 2.96$ GPa for RR1000. For $\omega \lesssim 6$ the presence of the intrusion raises the ratio significantly above one

$$J_x(S_1) = \frac{(1-\nu)K_I^2}{2\mu}, \qquad J_x(S_2) = \frac{(1-\nu)k_I^2}{2\mu},$$
$$J_x(S_3) = \sigma_1 \Delta u. \tag{23}$$

When $\theta = 0$ we have $J_x(S_1) = J_x(S_2) + J_x(S_3)$. But when $\theta > 0$ we have $J_x(S_1) < J_x(S_2) + J_x(S_3)$. This is illustrated in Fig. 12. In this figure it is seen that for experimentally observed intrusion geometries the force $J_x(S_2) + J_x(S_3)$ does not change significantly. Also, when $\omega$ increases the force $J_x(S_2) + J_x(S_3)$ tends to $J_x(S_1)$ and, hence, the presence of the intrusion becomes increasingly negligible. In fact, only when

$\omega \lesssim 6$ the intrusion raises significantly the force on the crack tip and on the plastic zone.

## 5 Discussion

By comparing Figs. 4 and 7 it is seen that the normal stresses within the intrusion differ significantly, *even when there is no applied stress*, from a linear superposition of the stress fields of the isolated intrusion (7), and the unloaded crack. It highlights the point made in the Introduction, with reference to the work of Chan (2014), of the necessity of satisfying the boundary conditions of traction free surfaces in the crack and a constant normal stress in the plastic zone, when the normal stress within the intrusion is calculated.

Figures 7 and 8 show the variation of the normal stress within the intrusion subjected to different values of $\omega$ and to different intrusion semi-angles $\theta$, respectively. It is seen that for experimentally observed intrusion geometries there is always a positive stress concentration at the crack tip, which generates a tensile region inside the thickest part of the intrusion. This tensile stress decreases with distance from the crack tip and, when $\omega$ is sufficiently small, it becomes compressive, gradually becoming tensile again towards the intrusion tip. At the intrusion tip the normal stress is tensile and is approximately equal to $\sigma_1$. This behaviour of the normal stress indicates that at moderate values of $\omega$ ($\omega < 4$) the crack will penetrate the intrusion during crack growth.

Figure 9 shows the variation of the hydrostatic stress within the intrusion subjected to different applied loads. It is seen that when there is no applied load ($\omega = 0$) the gradient of the hydrostatic stress within the intrusion encourages the drift of oxygen vacancies from the intrusion tip towards the crack tip, and hence the diffusion of oxygen atoms in the opposite direction. The gradient is reduced to almost zero when $\omega = 4$ and when $\omega = 40$ its sign is reversed. This suggests that the intrusion will grow to a larger size when there is no applied load, which is supported by the experimental observations of Kitaguchi et al. (2013). In their work on RR1000, the intrusions at static crack tips were examined following two loading conditions each for 5 h at $650\,°C$ in an oxidising environment. One of the loads was close to zero, and the other was slightly less than the threshold for crack-growth. The intrusion formed under almost zero load was significantly longer. In contrast,

Evans et al. (2013) suggested that oxygen diffusion is dominated by the stress at the ends of the intrusion (i.e. $x = 0$ and $x = l$). But in Fig. 9 we see that if that were true the growth of the intrusion would be independent of the applied load. We conclude that the origin of the enhancement of oxygen diffusion in SAGBO is primarily the gradient of the hydrostatic stress within the intrusion, and not the hydrostatic stresses at the ends of the intrusion.

The local stress intensity factor $k_I$, normalised to the applied stress intensity factor $K_I$, is shown in Fig. 10 as a function of $\omega$ for four values of the intrusion semi-angle $\theta$. Since an intrusion raises the local stress intensity factor above that of the DFZ-model, which corresponds to $\theta = 0$, it follows that the intrusion always provides an additional tensile load on the crack tip. This additional tensile load is clearly visible in the region $-2l \lesssim x \leq 0$ of Fig. 4. The force acting to advance the crack tip, as determined by $J_x(S_2)$ in (23), is proportional to $k_1^2$, and therefore it is also raised by the presence of the intrusion.

If we adopt the fracture criterion that $k_I$ has to exceed a critical value then as we increase the applied load from zero, fracture of the intrusion will occur so long as $k_I$ exceeds the critical value. As the crack grows from $c$ to $c + \delta c$, it penetrates the intrusion by $\delta c$ and the effective length $l$ of the intrusion decreases to $l - \delta c$. At a given applied stress $\sigma$ and yield stress $\sigma_1$, the variable $\omega$ then increases because $\delta \omega \approx (\omega/(2l))\delta c$, where the approximation assumes $c \gg l$. Thus if $\delta c > 0$ then $\delta \omega > 0$ for constant values of $\sigma$ and $\sigma_1$.

That $k_I$ decreases with increasing $\omega$ may be seen by writing $k_I$ in (22) as $k_I = \sigma_1 \sqrt{2\pi l}\ \tilde{k}_I(\omega)$. Then we obtain:

$$\left(\frac{\partial k_I}{\partial \omega}\right)_{\theta,\sigma,\sigma_1} = \frac{\sigma_1 \sqrt{2\pi l}}{\omega} \left[ \omega \left(\frac{\partial \tilde{k}_I}{\partial \omega}\right)_{\theta,\sigma,\sigma_1} - \tilde{k}_I \right], \quad (24)$$

where the partial derivatives are evaluated at constant semi-angle $\theta$ of the intrusion, constant applied load $\sigma$ and constant yield stress $\sigma_1$. In Fig. 13 we see that the term in the square brackets of (24) is negative for $\omega \geq 0$ for each value of $\theta$. Since the pre-factor $\sigma_1 \sqrt{2\pi l}/\omega$ is always positive it follows that $k_I$ always decreases with increasing $\omega$, that is with increasing crack length at constant applied load, yield stress and intrusion semi-angle. The crack may be arrested inside the intrusion if $k_I$ falls below the critical value.

It follows that if the crack is arrested inside the intrusion further crack growth will resume only when
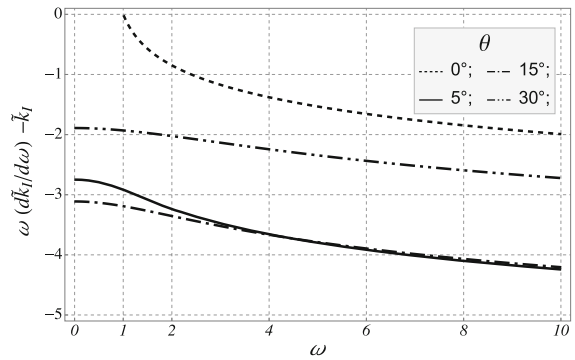


**Fig. 13** To show that the term in square brackets in (24) is always negative for $\omega \geq 0$

the intrusion has grown by further oxidation, thereby increasing $l$ and raising $k_I$ above the critical value. Thus, we may envisage steady-state crack growth with the crack tip always inside the intrusion, where the rate of crack growth is equal to the rate of growth of the oxide intrusion ahead of the crack.

Evans et al. (2013) stated that fracture of the intrusion in RR1000 occurs when $k_I$ reaches approximately 10 MPa m$^{1/2}$, about an order of magnitude larger than the typical critical stress intensity factors for oxides of the metals present in the superalloy. They attributed this observation to *compressive* stresses inside the intrusion just ahead of the crack. However, we have seen in Fig. 4 that the intrusion loads the crack in tension. And, as seen in Fig. 7 this tensile loading creates a *tensile* stress singularity just ahead of the crack, even when there is no externally applied load. We suggest the increased fracture toughness of the oxide intrusion, as compared with bulk samples of oxide material, originates from the plastic zone, which exists even when there is no externally applied load.

The extent to which the intrusion embrittles the material, by raising the force on the crack tip and on the plastic zone, is governed by $\omega$. As $\omega$ increases the plastic zone increases in size, screening and blunting the crack tip, which brings about the decrease of $k_I/K_I$ with increasing $\omega$ in Fig. 10. The intrusion then has a smaller influence on the stresses at the crack tip. Conversely, as the intrusion grows through oxidation, so that $\omega$ decreases, it begins to increase the force on the crack tip and on the plastic zone. As seen in Fig. 12 the intrusion begins to have a marked influence on both the crack tip and the plastic zone when $\omega \lesssim 6$. This requirement leads to the following approximate relation for the length of the intrusion when it begins to have a signif-

icant influence on the crack and plastic zone:

$$\frac{l}{c} \gtrsim \frac{\sigma^2}{70\sigma_1^2}. \tag{25}$$

# 6 Conclusions

A mathematical model has been developed to provide physical insight into the embrittlement of a long elastic–plastic crack by a relatively small, misfitting inclusion through functional relationships. In particular, we addressed the important example of the embrittlement of the Ni-based superalloys RR1000 at 650 °C caused by an oxide intrusion.

The dimensionless parameter $\omega = (\sigma/\sigma_1)/\sqrt{c/(2l)}$ emerges from the analysis, where $\sigma$ is applied normal stress, $\sigma_1$ is the yield stress, $c$ is the crack length, and $l$ is the length of the intrusion. This variable is key to understanding the embrittlement caused by the intrusion. We find the intrusion has a marked influence only when $\omega \lesssim 6$. At larger values of $\omega$ the intrusion is too small to have a detrimental effect on the fracture toughness of the alloy.

The intrusion is always 'anti-shielding', adding to a tensile applied load on the crack tip. Even in the absence of an externally applied load the tensile load on the crack tip arising from the intrusion creates a square root singularity in the stress field at the crack. In turn this singularity exceeds the compressive normal stress that exists within the thickest part of the intrusion when it is isolated, making it tensile. As a result, the intrusion fails near the crack tip because it is the region where the tensile stress is highest. When the crack advances into the intrusion the local stress intensity factor $k_I$ on the crack tip decreases with increasing crack length, because the effective length $l$ of the intrusion decreases raising $\omega$ and lowering $k_I$. Thus, it is possible that this reduction arrests the crack advance inside the intrusion. In that case we may envisage a steady state where the rate of crack growth is equal to the rate of growth of the intrusion ahead of the crack, and the plastic zone is continuously regenerated ahead of the intrusion. As a result of the anti-shielding effect of the intrusion both the local stress intensity factor $k_I$ and the length of the plastic zone, are increased compared to the case where the intrusion is replaced by a dislocation free zone of the same length. Similarly, the crack tip opening displacement $\Delta u$ is increased. Although the intrusion embrittles the medium, the fracture toughness is larger than that of the bulk oxide because the plastic zone ahead of the intrusion shields the crack tip.

The experimental observations of Kitaguchi et al. (2013) and Fig. 9 support the view that it is the gradient of the hydrostatic stress within the intrusion that is responsible for the enhancement of oxygen diffusion through the intrusion, and hence the increased rate of growth of the intrusion.

## Appendix: Definitions of the elliptic integrals

Let $m$ be the parameter, $n$ the characteristic, and $\phi$ the amplitude. The definitions used in this paper of the incomplete elliptic integrals of the first kind, $F(\phi|m)$, second kind, $E(\phi|m)$, and third kind, $\Pi(n; \phi|m)$, are as follows:

$$F(\phi|m) = \int_0^\phi \frac{d\theta}{\sqrt{1 - m\sin^2\theta}}, \tag{26a}$$

$$E(\phi|m) = \int_0^\phi d\theta \sqrt{1 - m\sin^2\theta}, \tag{26b}$$

$$\Pi(n; \phi|m) = \int_0^\phi \frac{d\theta}{(1 - n\sin^2\theta)\sqrt{1 - m\sin^2\theta}}. \tag{26c}$$

These definitions correspond to those in Abramowitz and Stegun (1972), where properties of the elliptic integrals may be found. $m$ and $n$ are usually real numbers between 0 and 1. The amplitude $\phi$ can be a complex number. When $\phi = \pi/2$, the elliptic integrals are called complete. The complete elliptic integrals of the first kind, $K(m)$, second kind, $E(m)$, and third kind, $\Pi(n|m)$, are then respectively:

$$K(m) = \int_0^{\pi/2} \frac{d\theta}{\sqrt{1 - m\sin^2\theta}}, \tag{27a}$$

$$\mathrm{E}\,(m) = \int_0^{\pi/2} d\theta\, \sqrt{1 - m \sin^2\theta}, \tag{27b}$$

$$\Pi\,(n|m) = \int_0^{\pi/2} \frac{d\theta}{(1 - n \sin^2\theta)\sqrt{1 - m \sin^2\theta}}. \tag{27c}$$

# References

Abramowitz M, Stegun IA (eds) (1972) Chapter 17 in Handbook of mathematical functions, 9th printing. Dover, New York, pp 587–607

Andrieu E, Molins R, Ghonem H, Pineau A (1992) Intergranular crack tip oxidation mechanism in a nickel-based superalloy. Mater Sci Eng A 154:21–28

Bache MR, Evans WJ, Hardy MC (1999) The effects of environment and loading waveform on fatigue crack growth in Inconel 718. Int J Fatigue 21:S69–S77

Bilby BA, Cottrell AH, Swinden KH (1963) The spread of plastic yield from a notch. Proc R Soc Lond A Math Phys Eng Sci 272:304–314

Chan KS (2014) Time-dependent crack growth thresholds of Ni-base superalloys. Metall Mater Trans A 45:3454–3466

Chang SJ, Ohr SM (1981) Dislocation−free zone model of fracture. J Appl Phys 52:7174–7181

Chang SJ, Ohr SM (1983) Distribution function of dislocations and condition of finite stress for the dislocation-free zone model of fracture. Int J Fracture 23:R3–R6

Cruchley S, Li HY, Evans HE, Bowen P, Child DJ, Hardy MC (2015a) The role of oxidation damage in fatigue crack initiation of an advanced Ni-based superalloy. Int J Fatigue 81:265–274

Cruchley S, Taylor MP, Li HY, Evans HE, Bowen P, Child DJ, Hardy MC (2015b) Effect of prior oxidation on high cycle fatigue performance of RR1000 and role of oxidation in fatigue crack initiation. Mater High Temp 32:68–73

Cruchley S, Evans H, Taylor M (2016) An overview of the oxidation of Ni-based superalloys for turbine disc applications: surface condition, applied load and mechanical performance. Mater High Temp 33:465–475

Dugdale DS (1960) Yielding of steel sheets containing slits. J Mech Phys Solids 8:100–104

Eshelby JD (1951) The force on an elastic singularity. Philos Trans R Soc Lond A 244:87–111

Eshelby JD (1956) The continuum theory of lattice defects. Solid State Phys 3:79–144

Evans HE (1995) Stress effects in high temperature oxidation of metals. Int Mater Rev 40:1–40

Evans HE, Li HY, Bowen P (2013) A mechanism for stress-aided grain boundary oxidation ahead of cracks. Scr Mater 69:179–182

Hörnqvist M, Viskari L, Moore KL, Stiller K (2014) High-temperature crack growth in a Ni-base superalloy during sustained load. Mater Sci Eng A 609:131–140

Karabela A, Zhao LG, Lin B, Tong J, Hardy MC (2013) Oxygen diffusion and crack growth for a nickel-based superalloy under fatigue-oxidation conditions. Mater Sci Eng A 567:46–57

Kitaguchi HS, Li HY, Evans HE, Ding RG, Jones IP, Baxter G, Bowen P (2013) Oxidation ahead of a crack tip in an advanced Ni-based superalloy. Acta Mater 61:1968–1981

Kitaguchi HS, Moody MP, Li HY, Evans HE, Hardy MC, Lozano-Perez S (2015) An atom probe tomography study of the oxide-metal interface of an oxide intrusion ahead of a crack in a polycrystalline Ni-based superalloy. Scr Mater 97:41–44

Knowles DM, Hunt DW (2002) The influence of microstructure and environment on the crack growth behavior of powder metallurgy nickel superalloy RR1000. Metall Mater Trans A 33:3165–3172

Krupp U (2005) Dynamic embrittlement—time-dependent quasi-brittle intergranular fracture at high temperatures. Int Mater Rev 50:83–97

Lardner RW (1974) Mathematical theory of dislocations and fracture. University of Toronto Press, Toronto

Li HY, Sun JF, Hardy MC, Evans HE, Williams SJ, Doel TJ, Bowen P (2015) Effects of microstructure on high temperature dwell fatigue crack growth in a coarse grain PM nickel based superalloy. Acta Mater 90:355–369

Liu HW, Oshida Y (1986) Grain boundary oxidation and fatigue crack growth at elevated temperatures. Theor Appl Fract Mech 6:85–94

Majumdar BS, Burns SJ (1983) A Griffith crack shielded by a dislocation pile-up. Int J Fracture 21:229–240

McMahon CJ, Coffin LF (1970) Mechanisms of damage and fracture in high-temperature, low-cycle fatigue of a cast nickel-based superalloy. Metall Mater Trans B 1:3443–3450

Németh AA, Crudden DJ, Collins DM, Armstrong DE, Reed RC (2016) Novel techniques to assess environmentally-assisted cracking in a nickel-based superalloy. In: Superalloys 2016: proceedings of the 13th international symposium of superalloys. Wiley, pp 801–810

Németh AA, Crudden DJ, Armstrong DE, Collins DM, Li K, Wilkinson AJ, Grovenor CR, Reed RC (2017) Environmentally-assisted grain boundary attack as a mechanism of embrittlement in a nickel-based superalloy. Acta Mater 126:361–371

Ohr SM, Chang SJ (1982) Dislocation−free zone model of fracture comparison with experiments. J Appl Phys 53:5645–5651

Pineau A, Antolovich SD (2009) High temperature fatigue of nickel-base superalloys—a review with special emphasis on deformation modes and oxidation. Eng Failure Anal 16:2668–2697

Rice JR (1968) A path independent integral and the approximate analysis of strain concentration by notches and cracks. J Appl Mech 35:379–386

Viskari L, Hörnqvist M, Moore KL, Cao Y, Stiller K (2013) Intergranular crack tip oxidation in a Ni-base superalloy. Acta Mater 61:3630–3639

Weertman J, Lin IH, Thomson R (1983) Double slip plane crack model. Acta Metall 31:473–482